ACS APPLIED MATERIALS & INTERFACES

Research Article

www.acsami.org

Three-Dimensional Hierarchical Frameworks Based on MoS_2 Nanosheets Self-Assembled on Graphene Oxide for Efficient Electrocatalytic Hydrogen Evolution

Weijia Zhou,*[,†] Kai Zhou,[†] Dongman Hou,[‡] Xiaojun Liu,[†] Guoqiang Li,[‡] Yuanhua Sang,[§] Hong Liu,[§] Ligui Li,[†] and Shaowei Chen*[,†,∥]

[†]New Energy Research Institute, School of Environment and Energy, South China University of Technology, Guangzhou Higher Education Mega Center, Guangzhou, Guangdong 510006, China

[‡]School of Materials Science and Engineering, South China University of Technology, Wushan Road, Tianhe District, Guangzhou, Guangdong 510006, China

[§]State Key Laboratory of Crystal Materials, Center of Bio & Micro/Nano Functional Materials, Shandong University, 27 Shandanan Road, Jinan, Shandong 250100, China

[∥]Department of Chemistry and Biochemistry, University of California, 1156 High Street, Santa Cruz, California 95064, United States

Supporting Information

ABSTRACT: Advanced materials for electrocatalytic water splitting are central to renewable energy research. In this work, three-dimensional (3D) hierarchical frameworks based on the self-assembly of MoS_2 nanosheets on graphene oxide were produced via a simple one-step hydrothermal process. The structures of the resulting 3D frameworks were characterized by using a variety of microscopic and spectroscopic tools, including scanning and transmission electron microscopies, X-ray diffraction, X-ray photoelectron spectroscopy, and Raman scattering. Importantly, the three-dimensional MoS_2/graphene frameworks might be used directly as working electrodes which exhibited apparent and stable electrocatalytic activity in hydrogen evolution reaction (HER), as manifested by a large cathodic current density with a small overpotential of −107 mV (−121 mV when loaded on a glassy-carbon electrode) and a Tafel slope of 86.3 mV/dec (46.3 mV/dec when loaded on a glassy-carbon electrode). The remarkable performance might be ascribed to the good mechanical strength and high electrical conductivity of the 3D frameworks for fast charge transport and collection, where graphene oxide provided abundant nucleation sites for MoS_2 deposition and oxygen incorporation led to the formation of defect-rich MoS_2 nanosheets with active sites for HER.

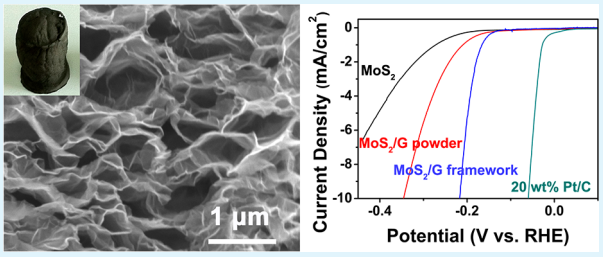

KEYWORDS: *MoS_2 nanosheet, graphene oxide, hydrothermal, three-dimensional framework, electrocatalytic, hydrogen evolution reaction*

INTRODUCTION

Hydrogen has been hailed as a promising alternative and renewable energy source that may replace fossil fuels in the future. Toward this end, one effective approach to hydrogen production is based on environmentally friendly electrochemical water-splitting.[1−3] In these studies, advanced catalysts for the hydrogen evolution reaction (HER) are generally needed to reduce overpotential and increase energy efficiency.[4,5] To date, the most effective electrocatalysts for HER are based on Pt-group metals, which are capable of catalyzing HER at a significant rate with almost no overpotential.[6,7] However, their scarcity and high costs have inhibited large-scale applications, and it remains a great challenge to develop highly active HER catalysts based on earth-abundant materials with a low overpotential. Since the report by Hinnemann et al.[8] that MoS_2 nanoparticles were active HER catalysts, the interest in using MoS_2 and related metal sulfides as water-splitting electrocatalysts has been intensified, and extensive research efforts have been devoted toward the enhancement of the catalytic activity by, for instance, loading catalysts on conductive substrates (e.g., graphene-protected 3D Ni foams and graphene nanosheets)[9−12] and enhanced exposure of active edges.[13−15] For instance, MoS_2 nanoparticles have been grown on reduced graphene oxide nanosheets (MoS_2/G) via a facile solvothermal procedure and the resulting composites exhibited excellent HER activity with a small overpotential of −100 mV, large cathodic currents, and a Tafel slope as small as 41 mV/dec.[10]

In fact, a large surface area and high electrical conductivity of the MoS_2-based HER electrocatalysts represent two important

Received: September 23, 2014
Accepted: October 27, 2014
Published: October 27, 2014

factors that are the key to the enhancement and optimization of the catalytic activity. 3D graphene frameworks with a high surface area and good electrical conductivity are good support materials for HER electrodes, which have been prepared previously by chemical vapor deposition (CVD),[16,17] hydrothermal processes,[18−21] and thermolysis.[22] However, it remains a great challenge to prepare highly efficient and low-cost composite 3D graphene frameworks and, in particular, to use them directly as binder-free HER electrodes, in contrast to the conventional methods[11,21] where Nafion is used as a binder to immobilize catalysts on an electrode surface. This is the primary motivation of the present study.

Within this context, herein we described the preparation of 3D hierarchical frameworks by the self-assembly of MoS_2 nanosheets on graphene oxide via a simple one-step hydrothermal process. The defect-rich MoS_2 nanosheets possessed an enlarged interlayer spacing due to oxygen incorporation from graphene oxides nanosheets. The resulting hierarchical frameworks might be used directly as binder-free working electrodes that exhibited efficient and stable electrocatalytic activity in HER, as manifested by a large cathodic current density with a small overpotential as low as −107 mV and a Tafel slope of 86.3 mV/dec.

EXPERIMENTAL SECTION

Materials. All reagents were of analytical grade and used without further purification. Ammonium molybdate ($(NH_4)_6Mo_7O_{24}\cdot 4H_2O$), thioacetamide ($C_2H_5NS$, TAA), graphite powders, sulfuric acid (H_2SO_4), sodium nitrate ($NaNO_3$), and potassium permanganate ($KMnO_4$) were obtained from Sinopharm Chemical Reagents Beijing Co. Water was supplied with a Barnstead Nanopure Water System (18.3 MΩ·cm).

Synthesis of Graphene Oxide. Graphene oxide was prepared by acid oxidation of graphite powders according to the modified Hummers' method.[23] Briefly, graphite (3.0 g) was added to concentrated sulfuric acid (70 mL) under magnetic stirring at room temperature, into which was added sodium nitrate (1.5 g) and the mixture was cooled to 0 °C. Under vigorous agitation, potassium permanganate (9.0 g) was added slowly while the temperature of the solution was kept below 20 °C. The reaction mixture was then incubated in a 40 °C water bath for 30 min, forming a thick paste. Then, 140 mL of Nanopure water was added, and the solution was stirred for another 15 min. An additional 500 mL of water was added, followed by a slow addition of 20 mL of H_2O_2 (30%), turning the color of the solution from brown to yellow. The mixture was filtered and washed with a 1:10 HCl aqueous solution (250 mL) to remove metal ions, followed by repeated washing with water and centrifugation to remove excessive acid. The resulting solids were dispersed in water by ultrasonication for 1 h at a concentration of 10 mg/mL.

Synthesis of 3D MoS_2 Nanosheets/Graphene Frameworks. 3D MoS_2 nanosheets/graphene hydrogels were prepared by a simple one-step hydrothermal process by adopting the procedures for the preparation of graphene hydrogels[18] and MoS_2 nanosheets.[17] Briefly, to prepare MoS_2 nanosheets/graphene (MoS_2/G) hydrogel at a mass ratio of 2:5, 26.5 mg of ammonium molybdate and 60 mg of thioacetamide were dissolved in 20 mL of a 3 mg/mL graphene oxide aqueous dispersion to form a homogeneous solution. The solution was transferred to a 25 mL Teflon-lined stainless steel autoclave and then heated in an electric oven at 200 °C for 24 h. The autoclave was naturally cooled to room temperature and the as-prepared 3D MoS_2 nanosheets/graphene hydrogels were removed with a pair of tweezers, washed with distilled water, and freeze-dried into an aerogel for further use. The 3D MoS_2 nanosheets/graphene frameworks at other MoS_2 loadings (mass ratio of MoS_2 and graphene at 1:4, 2:5, 11:20, 7:10, and 1:1) were synthesized in a similar manner. For comparison, MoS_2/G (2:5) nanopowders were also prepared via the same hydrothermal process except that the concentration of the aqueous dispersion of graphene oxide was only 0.2 mg/mL such that no 3D framework was formed. In addition, pure MoS_2 nanosheets were synthesized under the same conditions but without the addition of graphene oxide.

Characterizations. Field-emission scanning electron microscopic (FESEM, Model JSM-7600F) measurements were employed to characterize the morphologies of the obtained samples. Transmission electron microscopic (TEM) measurements were carried out with a JEOL JEM 2100F microscope. Powder X-ray diffraction (XRD) patterns of the samples were recorded with a Bruke D8 Advance powder X-ray diffractometer with Cu Kα (λ = 0.15406 nm) radiation. X-ray photoelectron spectroscopic (XPS) measurements were performed using an ESCALAB 250 spectrometer. Raman spectra were recorded on a RENISHAW inVia instrument with an Ar laser source of 488 nm in a macroscopic configuration. BET surface areas were characterized by Micromeritics ASAP 2010 with nitrogen adsorption at 77 K and the Barrett−Joyner−Halenda (BJH) method.

Electrochemistry. Electrochemical measurements were performed with an electrochemical workstation (Solartron Analytical 1287 + 1260) in a 0.5 M H_2SO_4 aqueous solution. A saturated calomel electrode ($Hg/HgCl_2$ in saturated KCl) and a platinum wire were used as the reference and counter electrode, respectively. The MoS_2/G 3D frameworks were cut into small pieces and used as working electrodes. The current densities were evaluated in terms of the total mass of the MoS_2/G electrodes.

Comparative studies were also carried out by loading the catalysts, such as MoS_2/G 3D frameworks, MoS_2/G (2:5) powders, graphene oxide, and 20 wt % Pt/C, on a glassy carbon electrode. Experimentally, 4 mg of the respective catalyst powders was dispersed in 1 mL of 4:1 (v/v) water/ethanol mixed solvents with 40 μL of a Nafion solution under ultrasonication for 30 min. A 4 μL portion of the resulting solution was dropcast onto the glassy-carbon disk by a microliter syringe and dried at room temperature. The catalyst loadings were all 0.22 mg/cm^2.

The polarization curves were obtained by sweeping the potential from 0 to −0.8 V (vs SCE) at a potential sweep rate of 5 mV/s. The accelerated stability tests were performed in 0.5 M H_2SO_4 at room temperature by potential cycling between +0.1 and −0.5 V (vs SCE) at a sweep rate of 100 mV/s for a given number of cycles. Current−time responses were monitored by chronoamperometric measurements for up to 8 h. Hydrogen production at the electrodes was carried out at −0.4 V (vs SCE), and the rate of hydrogen gas production was quantified by gas chromatographic measurements (GC-2060F, LuNan Analytical Instruments, LTD, China). Experimentally, the gas generated from the sealed electrolytic cell was injected into the gas chromatography instrument by the continuous sample inlet system (with N_2 as the carrier gas) at a sampling interval of 1 point per 10 min. The hydrogen production rate was quantified by calibration of the integrated peak areas against the standard value of 1 mL of 99.999% H_2.

In all measurements, the SCE reference electrode was calibrated with respect to a reversible hydrogen electrode (RHE). The calibration was performed in a high purity H_2 (99.999%) saturated electrolyte with two Pt wires as the working electrode and counter electrode, respectively. Cyclic voltammograms (CVs) were acquired at the scan rate of 1 mV/s, and the average of the two potentials at which the current crossed zero was taken as the thermodynamic potential for the hydrogen electrode reactions. In 0.5 M H_2SO_4, E(SCE) = E(RHE) + 0.164 V (Figure S1).

RESULTS AND DISCUSSION

The MoS_2/G hierarchical framework hydrogels were prepared by simple one-step hydrothermal heating of a homogeneous aqueous dispersion containing graphene oxide, ammonium molybdate, and thioacetamide at 200 °C for 24 h (Figure 1a). As shown in Figure 1b and c, the MoS_2/G freeze-dried aerogel exhibit a well-defined and interconnected porous network. The pore diameters range from submicrometers to several micrometers, and the pore walls consist of stacked graphene oxide

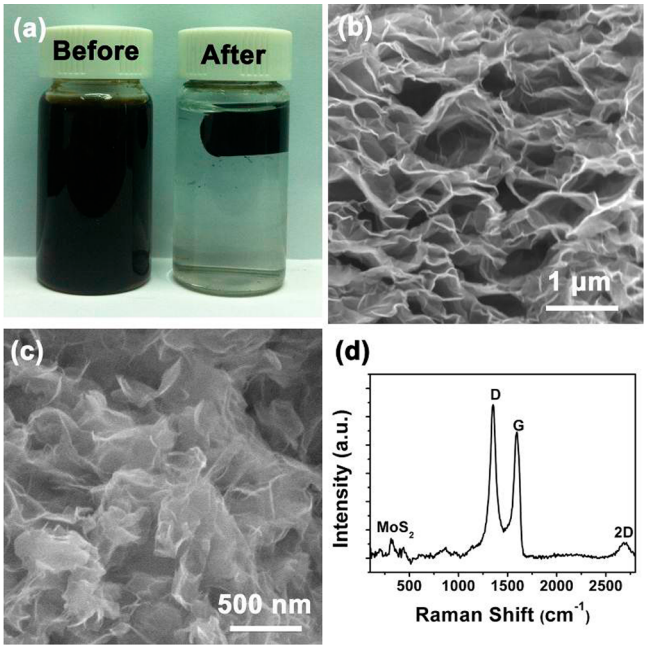

Figure 1. (a) Photographs of a homogeneous aqueous dispersion containing graphene oxide, ammonium molybdate, and thioacetamide (left) before and (right) after hydrothermal reduction at 200 °C for 24 h. (b, c) SEM images and (d) Raman spectrum of the resulting MoS_2/G (2:5) hierarchical framework.

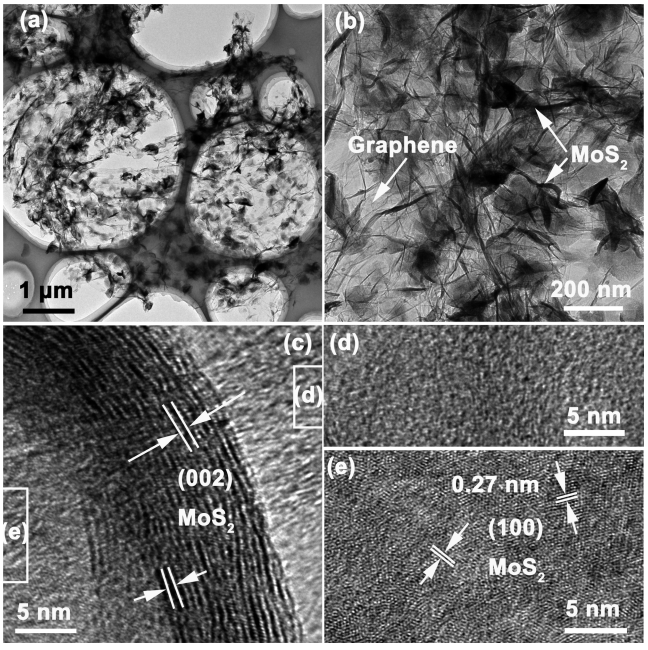

Figure 2. Representative TEM images of (a–c) the MoS_2/G (2:5) frameworks, (d) graphene nanosheets, and (e) MoS_2 nanosheets.

sheets and MoS_2 nanosheets, as revealed in EDS studies where the MoS_2/G hierarchical framework was found to be composed of C, Mo, and S elements (Figure S2). Such a 3D hierarchical framework was found to possess a high specific surface area and electrical conductivity. The corresponding BET results (Figure S3) show that there are similar BET values between the MoS_2/G (2:5) hierarchical framework and pure graphene hydrogel at 149.3 and 147.5 m^2/g, respectively. This is probably because the ultrathin MoS_2 nanosheets possess a high surface area and limit the restacking of graphene sheets by $\pi-\pi$ interactions.[24,25] Raman spectroscopic studies further confirmed the formation of a hierarchical nanocomposite framework. From Figure 1d, one can see that the D, G, and 2D vibrational bands of graphene oxide can be clearly identified at 1351, 1598, and 2698 cm^{-1} respectively; and the vibrational band at 313.5 cm^{-1} is characteristic of MoS_2.[10]

Further structural insights were obtained in TEM studies, as depicted in Figure 2. One can see that ripples and corrugations are rather well-defined, revealing the ultrathin nature of the graphene and MoS_2 nanosheets (Figure 2a and b) with MoS_2 represented by the dark-contrast objects whereas graphene oxide by the gray background; and the layered structures can be clearly seen in high-resolution TEM studies with an interlayer spacing of about 0.8 nm (Figure 2c), which is somewhat larger than 0.6 nm between the (002) crystal planes of pure MoS_2 (JCPDS No. 73-1508). This is possibly due to the incorporation of oxygen from graphene oxide nanosheets into MoS_2 that weakened the interlayer interactions and steric contributions of the three-dimensional graphene frameworks.[15] Furthermore, on the surface of the MoS_2 nanosheets one can see a defect-rich structure with nanodomains of short-range ordering, with an interlayer spacing of 0.27 nm that corresponds to the (100) crystal planes of MoS_2 (Figure 2e). The exposed molybdenum edges are likely the active sites for HER (vide infra).[15,26,27] In contrast, no lattice phases were observed with the graphene nanosheets (Figure 2d).

X-ray photoelectron spectroscopic (XPS) measurements were then carried out to further investigate the chemical composition and valence states of the MoS_2/G nanocomposite frameworks. From the survey spectrum in panel a of Figure 3,

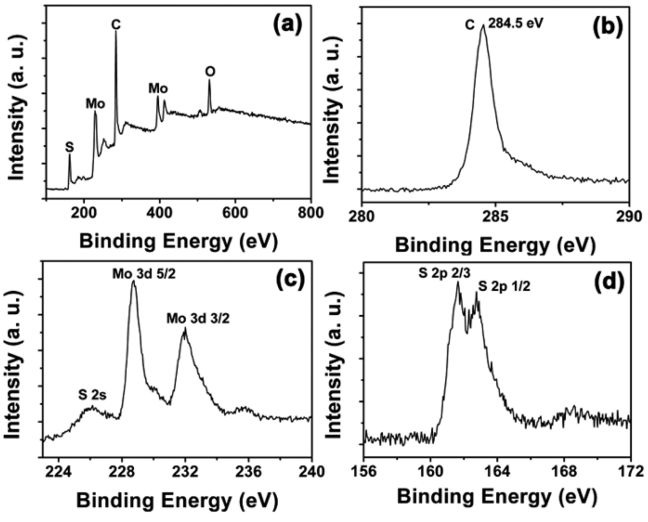

Figure 3. (a) XPS survey spectrum and high-resolution scans for the (b) C 1s, (c) Mo 3d, and (d) S 2p electrons of MoS_2/G (2:5).

the elements of Mo, C, O, and S can be clearly identified. Figure 3b shows the C 1s characteristic peak at 284.5 eV which is consistent with the sp^2 carbon of the graphene (oxide) scaffold. Figure 3c and d depicts the high-resolution scans of the Mo 3d, S 2p, and S 2s electrons, with the characteristic peaks for Mo^{4+} at 228.7 and 232 eV and those for S^{2-} at 161.6, 162.7, and 226 eV, again, signifying the formation of MoS_2 in the 3D frameworks.

dx.doi.org/10.1021/am506545g | ACS Appl. Mater. Interfaces 2014, 6, 21534–21540

Note that during hydrothermal treatments, three-dimensional random stacking between flexible graphene sheets most likely occurred because of the hydrophobic and π-interactions between the graphene oxide nanosheets;[18] concurrently, MoS_2 nanosheets were produced from ammonium molybdate and thioacetamide and self-assembled onto the graphene oxide surfaces. Stable MoS_2/G aerogels were obtained after the freeze-dried process, as shown in Figure 4a. The corresponding

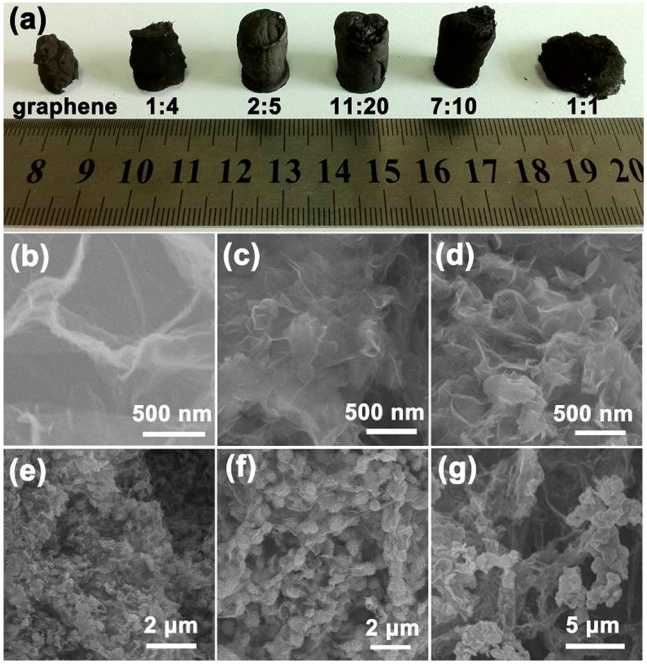

Figure 4. (a) Photographs and SEM images of MoS_2/G hierarchical frameworks at different MoS_2 loadings: (b) pure graphene frameworks, (c) 1:4, (d) 2:5, (e) 11:20, (f) 7:10, and (g) 1:1.

morphologies, structures, and composition of the 3D hierarchical frameworks at different MoS_2 loadings were examined by SEM and EDS studies (Figure 4b–g and Figure S4), where one can see that the eventual MoS_2 loadings were in good agreement with the initial feed ratios and the aerogel structures depend strongly on the mass ratio between graphene oxide and MoS_2. For instance, at the MoS_2 loadings up to 7:10, mechanically robust MoS_2/G hierarchical frameworks were obtained; and in the intermediate range of MoS_2 loadings (2:5 and 11:20), the resulting MoS_2/G 3D frameworks exhibited a more rigid structure than those at lower MoS_2 contents (pure graphene and 1:4). This is possibly due to the bonding interactions between cations and graphene oxide nanosheets. Similar results have been reported previously where Fe^{3+} ions were found to induce the self-assembly of graphene oxide.[28] We also observed the condensation of graphene oxide sheets and ammonium molybdate in aqueous solutions into hydrogel at room temperature after 24 h (Figure S5). In contrast, when the MoS_2 content was increased to 1:1, no cross-linking of graphene oxide occurred because of blocking by the large-sized MoS_2 nanoparticles (Figure 4g), such that MoS_2/G hydrogels could not be produced (Figure 4a). In fact, MoS_2/G (1:1) exhibits a small BET specific surface area of only 28.4 m^2/g (Figure S6), much lower than that (149.3 m^2/g) of MoS_2/G (2:5), as a result of the large-size MoS_2 nanoparticles and the collapse of the 3D frameworks.

XRD studies were then carried out to examine the crystalline characteristics of the MoS_2/G hierarchical frameworks at different MoS_2 loadings. As depicted in panel a of Figure 5,

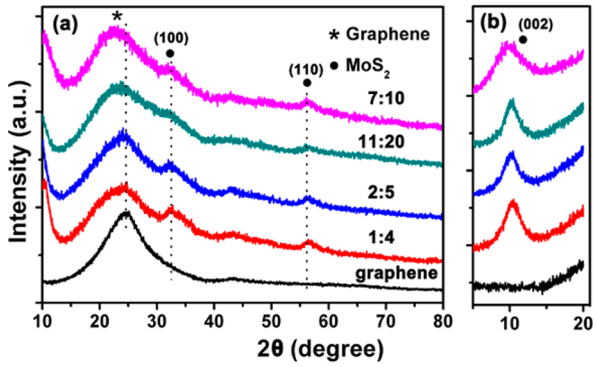

Figure 5. (a) XRD patterns of the MoS_2/G hierarchical frameworks at different MoS_2 loadings. (b) Zoom-in of the low-angle region of the XRD profiles.

for pure graphene oxide (black curve), a broad diffraction peak can be identified at 24.5°, corresponding to an interlayer spacing of 0.364 nm that is somewhat larger than that of the graphite (002) crystal planes. This indicates poor ordering of the graphene sheets along their stacking direction with only a few layers in the graphene oxide sheets. Interestingly, this peak position exhibited a clear decrease with increasing MoS_2 contents: 23.8° for 1:4 (red curve), 23.5° for 2:5 (blue curve), 22.9° for 11:20 (green curve), and 22.5° for 7:10 (magenta curve), suggesting increasing interlayer separation of the graphene (oxide) sheets likely because of the steric effect of MoS_2 nanosheets and/or effect of S-doping. Similar results have been reported where the interlayer spacings of graphene increased when the graphene was functionalized with oxygen or phosphate.[29,30] With the loading of various amounts of MoS_2, the MoS_2/G 3D frameworks exhibited three additional diffraction peaks at ca. 10.4°, 32.7°, and 56.5°, which may be assigned to the (002), (100), and (110) crystal planes of MoS_2, respectively. Note that the (002) diffraction of MoS_2 in the MoS_2/G 3D frameworks actually occurred at a somewhat smaller angle than pure MoS_2 (JCPDS No. 73-1508), signifying an enlarged interlayer spacing. In addition, detailed analysis in panel b shows that the (002) diffraction of all MoS_2/G 3D frameworks actually shifts to a lower angle. The calculated d spacings (0.85–0.90 nm) of MoS_2/G at various MoS_2 loadings are clearly greater than that of pristine 2H-MoS_2 (0.61 nm), suggesting the formation of a new lamellar structure. In fact, these XRD results suggested an enlarged (002) interlayer spacing which was consistent with the TEM data presented in Figure 2, likely due to the incorporation of oxygen from graphene oxides nanosheets and weakened interlayer interactions. Similar results have been reported by Xie et al.[15] where MoS_2 with an enlarged interlayer spacing of the (002) lattice planes was observed and oxygen incorporation was found to effectively regulate the electronic structures of the MoS_2 nanosheets. Moreover, two almost invariant diffractions at 32.7° and 56.5° for the MoS_2 (100) and (110) crystal planes indicates consistent atomic arrangements along the basal planes among the series of MoS_2/G nanocomposite frameworks.

The MoS_2/G hierarchical frameworks obtained above were then cut into small slices with a knife, and were used directly as electrodes without a binding agent and/or conducting additives

because of its high porosity, good conductivity, and excellent mechanical strength. Linear sweep voltammograms of the MoS_2/G electrodes are shown in Figure 6a. As can be seen,

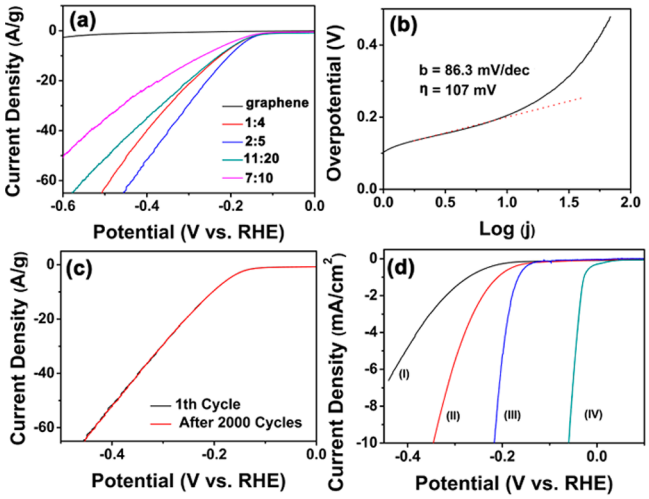

Figure 6. (a) Polarization curves of MoS_2/G 3D framework at different MoS_2 loadings. The currents were normalized to the total mass of the MoS_2/G catalysts. (b) Tafel plot for the MoS_2/G (2:5) framework electrode; (c) HER polarization curves for the MoS_2/G (2:5) framework electrode before and after 2000 cycles in the stability test. (d) Polarization curves for HER on a glassy-carbon electrodes modified with (I) pure MoS_2, (II) MoS_2/G (2:5) powders, (III) MoS_2/G (2:5) frameworks, and (IV) 20 wt % Pt/C, respectively.

pure graphene oxide frameworks (black curve) showed poor catalytic activity for HER, with virtually no cathodic currents even at potentials up to −0.6 V. In contrast, the MoS_2/G framework electrodes exhibited apparent cathodic currents at potentials more negative than about −0.107 V. This small overpotential (η) of 107 mV suggests superior HER activity, which is close to leading literature results, such as MoS_2 nanoparticles/graphene (100 mV),[10] MoS_2/graphene/Ni-foam (109 mV),[9] and defect-rich MoS_2 nanosheets (120 mV).[14] In addition, one can see from Figure 6a that at −0.4 V, the MoS_2/G electrode (2:5) exhibits the largest cathodic current density of 52.4 A/g, as compared to 40.4 A/g for 1:4, 34.9 A/g for 11:20, 24.0 A/g for 7:10, and 1.1 A/g for pure graphene. Moreover, the linear portion of the Tafel plots (Figure 6b) were fit to the Tafel equation ($\eta = b \log j + a$, where j is the current density and b is the Tafel slope). The Tafel slope was estimated to be 86.3 mV/dec for MoS_2/G (2:5). Note that this is close to or better than the records of MoS_2-based electrocatalysts (Table S1), such as MoS_2/graphene/Ni-foam (42.8 mV/dec),[9] MoS_2 films with vertically aligned layers (105−120 mV/dec),[13] and 3D MoS_2 sponges (175 mV/dec).[31]

It should be noted that in acidic media, three principal steps have been proposed for the conversion of H^+ to H_2, commonly referred to as the Volmer, Heyrovsky, and Tafel reactions, where the corresponding Tafel slopes are 120, 40, and 30 mV/dec, respectively.[9,13,32] The mechanism typically involves three major reactions,[32,33]

$$H_3O^+ + e{-}M \leftrightarrow H{-}M + H_2O \quad \text{(discharge reaction)} \tag{1}$$

$$2H{-}M \leftrightarrow H_2{-}M + M \quad \text{(combination reaction)} \tag{2}$$

$$H_3O^+ + e{-}M + H{-}M \leftrightarrow H_2{-}M + M + H_2O \quad \text{(ion + atom reaction)} \tag{3}$$

where e−M denotes metal-bound electrons and H−M and H_2−M represent a hydrogen atom and molecule adsorbed on to a surface metal atom, respectively. The Tafel slope of 86.3 mV/dec observed herein suggests that both the Volmer reaction, a discharge step that converted protons into absorbed hydrogen atoms on the catalyst surface, and the Heyrovsky reaction that involved the formation of surface-bound hydrogen molecules, played a significant role in determining the HER rate at the MoS_2/G (2:5) framework electrode.

In addition to good catalytic activity, the MoS_2/G electrodes also exhibited good stability for HER in acidic environments. Figure 6c shows that even after 2000 potential cycles, the j−V curve of the MoS_2/G (2:5) electrode remained almost invariant. The reverse scans between −0.34 and +0.26 V also confirmed good stability and high electrochemical area of the MoS_2/G electrode (Figure S7). This suggests strong bonding interactions between the MoS_2 nanosheets and the graphene oxide in the one-step hydrothermal procedure, which enabled fast electron transfer and collection.

Comparative studies were also carried out with other catalysts, where a calculated amount of the MoS_2/G framework nanocomposites, MoS_2/G powders, pure MoS_2, and 20 wt % Pt/C were cast onto a glassy-carbon electrode and subjected to voltammetric sweeps in 0.5 M H_2SO_4, as depicted in Figure 6d. One can see that the MoS_2/G (2:5) frameworks-modified electrode (curve III) exhibited a markedly higher cathodic current and lower overpotential than pure MoS_2 (curve I) and MoS_2/G (2:5) powders (curve II), although the overall performance was subpar as compared to that of 20 wt % Pt/C (curve IV). For instance, the overpotentials are 193.2, 154.1, 121.4, and 8.4 mV for pure MoS_2, MoS_2/G powders, MoS_2/G framework, and 20 wt % Pt/C, respectively. The corresponding Tafel slopes for pure MoS_2, MoS_2/G (2:5) powders, MoS_2/G (2:5) framework, and 20 wt % Pt/C were estimated to be 152.8, 58.1, 46.3, and 31.2 mV/dec, respectively (Figure S8). In comparison with the MoS_2/G powders, the enhanced HER performance of the MoS_2/G frameworks is likely due to the 3D framework structure, which exhibited a high electrochemical area for the diffusion of electrolyte ions. In fact, SEM studies showed a much rougher surface of the MoS_2/G frameworks-modified glassy-carbon electrode than that modified by MoS_2/G powders (Figure S9). This suggests a higher contact area of the MoS_2/G frameworks with electrolyte ions and thus a shorter ion diffusion path and faster charge transport. In additions, with a maximal loading of only 0.22 mg/cm^2 of the catalysts on the glassy carbon electrode surface (Figure S10), it is not ideal for practical applications. These results also highlight the significance of using the 3D MoS_2/G frameworks directly as working electrodes in enhancing the HER catalytic performance.

To further investigate the stability of the MoS_2/G hierarchical frameworks in HER, the cathodic currents of the MoS_2/G framework electrodes at the applied potential of −0.236 V were monitored for up to 1 h, as presented in Figure 7a. It can be seen that the MoS_2/G hierarchical framework (2:5) electrode exhibited the largest HER current of about 17.2 A/g among the series (in comparison, 15.1 A/g for 1:4, 11.4 A/g for 11:20, 8.3 A/g for 7:10, and 2.5 A/g for pure graphene); and the currents remained largely unchanged (similar behaviors

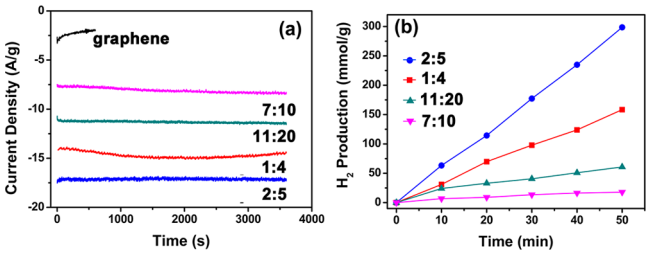

Figure 7. (a) Current−time responses of the MoS_2/G hierarchical frameworks at different MoS_2 loading at the applied potential of −0.236 V. (b) Production of hydrogen gas normalized by the weight of the MoS_2/G framework electrodes at different reaction times.

were observed even for over 8 h of continuous operation, Figure S11), suggesting excellent durability of the MoS_2/G hierarchical framework electrodes for HER. A number of bubbles were also observed on the surface of the MoS_2/G hierarchical framework electrode (Figure S12). The gas was confirmed to be hydrogen by gas chromatography measurements, and the amounts of hydrogen produced at the MoS_2/G hierarchical framework electrodes at different MoS_2 loadings are shown in Figure 7b. Linear regressions of the experimental data yield the corresponding hydrogen production rates which decrease in the order of 2:5 (358.2 mmol/g h) > 1:4 (189.5 mmol/g h) > 11:20 (72.7 mmol/g h) > 7:10 (21.5 mmol/g h). Again, this suggests that the MoS_2/G (2:5) 3D frameworks represent the best electrocatalysts for HER among the series. It is worth noting that stable MoS_2/G hydrogel (1:1) could not be produced and cut into small pieces as working electrodes. Thus, no HER data were obtained.

The high HER activity as well as good stability of the MoS_2/G hierarchical frameworks can be attributed to at least three factors. (i) Large conjugated structures of the graphene (oxide) 3D frameworks with continuously interconnected pores and a high surface-to-volume ratio provide abundant nucleation sites to form strong bindings with MoS_2 nanosheets, leading to fast interdomain electron transport. (ii) Good conductivity of the 3D graphene frameworks allows for effective charge collection and transfer, as revealed in electrochemical impedance spectroscopy (EIS) studies (Figure S13). More detailed analyses were carried out by fitting the impedance data to an equivalent circuit consisting of a series of a resistor and a capacitor. The internal resistances of the MoS_2/G hierarchical framework electrodes were found to be all very small within the narrow range of 1.78−2.46 Ω. The charge transfer resistance (R_{ct}) for the MoS_2/G hierarchical frameworks (2:5) was also very small at 2.52 Ω, close to that of pure graphene framework (1.85 Ω). At increasing loading of MoS_2, the R_{ct} values increased somewhat to, for example, 14.3 Ω for 11:20 and 18.7 Ω for 7:10. Additionally, in the low frequency region, a vertical straight line was evident suggesting that the 3D graphene frameworks (MoS_2 loading up to 11:20) exhibited facile ion diffusion. This confirms that the incorporation of the 3D graphene frameworks greatly enhanced charge transport, resulting in significant improvement of the HER performances. (iii) MoS_2 nanosheets that were grown on the surface of graphene oxide exhibited a high defect density due to the incorporation of oxygen from graphene oxide nanosheets that produced increasing molybdenum-edge catalyst sites. Because of the synergistic structural and electronic interactions, the MoS_2/G hierarchical frameworks displayed both rich active sites and high electrical conductivity, leading to enhanced HER activity.

CONCLUSIONS

Mechanically robust and electrically conductive MoS_2/G 3D hierarchical frameworks were prepared by a one-step hydrothermal process with an aqueous dispersion of graphene oxide, ammonium molybdate, and thioacetamide. The formation of nanocomposite frameworks was confirmed in SEM, TEM, XRD, XPS, and Raman measurements. The defect-rich MoS_2 nanosheets possessed an enlarged interlayer spacing due to the incorporation of oxygen from graphene oxides nanosheets that led to weakened interlayer interactions. Interestingly, blocks of the MoS_2/G hierarchical frameworks might be used directly as working electrodes and exhibited apparent and stable HER electrocatalytic activity. The best performance was observed with the frameworks at a MoS_2/G ratio of 2:5 that featured an overpotential of only −107 mV (in comparison to −121 mV when loaded on a GC electrode), a Tafel slope of 86.3 mV/dec (46.3 mV/dec when loaded on a GC electrode), and almost no change of the cathodic currents in HER for up to 8 h of continuous operation. This study highlights the significance of the formation of three-dimensional hierarchical frameworks based on the self-assembly of MoS_2 nanosheets on graphene oxide in the enhancement of HER electrocatalytic activity.

ASSOCIATED CONTENT

Supporting Information

EDS results, nitrogen adsorption/desorption isotherms, cyclic voltammograms, Tafel plots, SEM images, current−time plots, Nyquist plots, XRD data, and comparison of HER activity. This material is available free of charge via the Internet at http://pubs.acs.org.

AUTHOR INFORMATION

Corresponding Authors

*E-mail: eszhouwj@scut.edu.cn (W.Z.).
*E-mail: shaowei@ucsc.edu (S.C.).

Author Contributions

The manuscript was written through contributions of all authors. All authors have given approval to the final version of the manuscript.

Notes

The authors declare no competing financial interest.

ACKNOWLEDGMENTS

This work was supported by the National Recruitment Program of Global Experts, the PhD Start-up Funds of the Natural Science Foundation of Guangdong Province (S2013040016465), Zhujiang New Stars of Science & Technology (2014J2200061), and the Fundamental Research Funds for Central Universities (x2hjD2131690).

REFERENCES

(1) Anxolabéhère-Mallart, E.; Costentin, C.; Fournier, M.; Nowak, S.; Robert, M.; Savéant, J.-M. Boron-Capped Tris(glyoximato) Cobalt Clathrochelate as a Precursor for the Electrodeposition of Nanoparticles Catalyzing H2 Evolution in Water. *J. Am. Chem. Soc.* **2012**, *134*, 6104−6107.

(2) Subbaraman, R.; Tripkovic, D.; Strmcnik, D.; Chang, K.-C.; Uchimura, M.; Paulikas, A. P.; Stamenkovic, V.; Markovic, N. M. Enhancing Hydrogen Evolution Activity in Water Splitting by Tailoring Li+-Ni(OH)2-Pt Interfaces. *Science* **2011**, *334*, 1256−1260.

(3) Zhou, W.; Wu, X.-J.; Cao, X.; Huang, X.; Tan, C.; Tian, J.; Liu, H.; Wang, J.; Zhang, H. Ni3S2 Nanorods/Ni Foam Composite Electrode with Low Overpotential for Electrocatalytic Oxygen Evolution. *Energy Environ. Sci.* **2013**, *6*, 2921−2924.
(4) He, C.; Wu, X.; Shen, J.; Chu, P. K. High-Efficiency Electrochemical Hydrogen Evolution Based on Surface Autocatalytic Effect of Ultrathin 3C-SiC Nanocrystals. *Nano Lett.* **2012**, *12*, 1545−1548.
(5) Helm, M. L.; Stewart, M. P.; Bullock, R. M.; DuBois, M. R.; DuBois, D. L. A Synthetic Nickel Electrocatalyst with a Turnover Frequency Above 100,000 s−1 for H2 Production. *Science* **2011**, *333*, 863−866.
(6) Esposito, D. V.; Hunt, S. T.; Stottlemyer, A. L.; Dobson, K. D.; McCandless, B. E.; Birkmire, R. W.; Chen, J. G. Low-Cost Hydrogen-Evolution Catalysts Based on Monolayer Platinum on Tungsten Monocarbide Substrates. *Angew. Chem., Int. Ed.* **2010**, *122*, 10055−10058.
(7) Stephens, I. E. L.; Chorkendorff, I. Minimizing the Use of Platinum in Hydrogen-Evolving Electrodes. *Angew. Chem., Int. Ed.* **2011**, *50*, 1476−1477.
(8) Hinnemann, B.; Moses, P. G.; Bonde, J.; Jørgensen, K. P.; Nielsen, J. H.; Horch, S.; Chorkendorff, I.; Nørskov, J. K. Biomimetic Hydrogen Evolution: MoS2 Nanoparticles as Catalyst for Hydrogen Evolution. *J. Am. Chem. Soc.* **2005**, *127*, 5308−5309.
(9) Chang, Y.-H.; Lin, C.-T.; Chen, T.-Y.; Hsu, C.-L.; Lee, Y.-H.; Zhang, W.; Wei, K.-H.; Li, L.-J. Highly Efficient Electrocatalytic Hydrogen Production by MoSx Grown on Graphene-Protected 3D Ni Foams. *Adv. Mater.* **2013**, *25*, 756−760.
(10) Li, Y.; Wang, H.; Xie, L.; Liang, Y.; Hong, G.; Dai, H. MoS2 Nanoparticles Grown on Graphene: An Advanced Catalyst for the Hydrogen Evolution Reaction. *J. Am. Chem. Soc.* **2011**, *133*, 7296−7299.
(11) Liao, L.; Zhu, J.; Bian, X.; Zhu, L.; Scanlon, M. D.; Girault, H. H.; Liu, B. MoS2 Formed on Mesoporous Graphene as a Highly Active Catalyst for Hydrogen Evolution. *Adv. Funct. Mater.* **2013**, *23*, 5326−5333.
(12) Chang, Y.-H.; Nikam, R. D.; Lin, C.-T.; Huang, J.-K.; Tseng, C.-C.; Hsu, C.-L.; Cheng, C.-C.; Su, C.-Y.; Li, L.-J.; Chua, D. H. C. Enhanced Electrocatalytic Activity of MoSx on TCNQ-Treated Electrode for Hydrogen Evolution Reaction. *ACS Appl. Mater. Interfaces* **2014**, *6*, 17679−17685.
(13) Kong, D.; Wang, H.; Cha, J. J.; Pasta, M.; Koski, K. J.; Yao, J.; Cui, Y. Synthesis of MoS2 and MoSe2 Films with Vertically Aligned Layers. *Nano Lett.* **2013**, *13*, 1341−1347.
(14) Xie, J.; Zhang, H.; Li, S.; Wang, R.; Sun, X.; Zhou, M.; Zhou, J.; Lou, X. W.; Xie, Y. Defect-Rich MoS2 Ultrathin Nanosheets with Additional Active Edge Sites for Enhanced Electrocatalytic Hydrogen Evolution. *Adv. Mater.* **2013**, *25*, 5807−5813.
(15) Xie, J.; Zhang, J.; Li, S.; Grote, F.; Zhang, X.; Zhang, H.; Wang, R.; Lei, Y.; Pan, B.; Xie, Y. Controllable Disorder Engineering in Oxygen-Incorporated MoS2 Ultrathin Nanosheets for Efficient Hydrogen Evolution. *J. Am. Chem. Soc.* **2013**, *135*, 17881−17888.
(16) Chen, Z.; Ren, W.; Gao, L.; Liu, B.; Pei, S.; Cheng, H.-M. Three-Dimensional Flexible and Conductive Interconnected Graphene Networks Grown by Chemical Vapour Deposition. *Nat. Mater.* **2011**, *10*, 424−428.
(17) Zhou, W.; Yin, Z.; Du, Y.; Huang, X.; Zeng, Z.; Fan, Z.; Liu, H.; Wang, J.; Zhang, H. Synthesis of Few-Layer MoS2 Nanosheet-Coated TiO2 Nanobelt Heterostructures for Enhanced Photocatalytic Activities. *Small* **2013**, *9*, 140−147.
(18) Xu, Y.; Sheng, K.; Li, C.; Shi, G. Self-Assembled Graphene Hydrogel via a One-Step Hydrothermal Process. *ACS Nano* **2010**, *4*, 4324−4330.
(19) Hu, H.; Zhao, Z.; Wan, W.; Gogotsi, Y.; Qiu, J. Ultralight and Highly Compressible Graphene Aerogels. *Adv. Mater.* **2013**, *25*, 2219−2223.
(20) Huang, G.; Chen, T.; Chen, W.; Wang, Z.; Chang, K.; Ma, L.; Huang, F.; Chen, D.; Lee, J. Y. Graphene-Like MoS2/Graphene Composites: Cationic Surfactant-Assisted Hydrothermal Synthesis and Electrochemical Reversible Storage of Lithium. *Small* **2013**, *9*, 3693−3703.
(21) Hou, Y.; Zhang, B.; Wen, Z.; Cui, S.; Guo, X.; He, Z.; Chen, J. A 3D Hybrid of Layered MoS2/Nitrogen-Doped Graphene Nanosheet Aerogels: an Effective Catalyst for Hydrogen Evolution in Microbial Electrolysis Cells. *J. Mater. Chem. A* **2014**, *2*, 13795−13800.
(22) Qie, L.; Chen, W.; Xu, H.; Xiong, X.; Jiang, Y.; Zou, F.; Hu, X.; Xin, Y.; Zhang, Z.; Huang, Y. Synthesis of Functionalized 3D Hierarchical Porous Carbon for High-Performance Supercapacitors. *Energy Environ. Sci.* **2013**, *6*, 2497−2504.
(23) Hummers, W. S.; Offeman, R. E. Preparation of Graphitic Oxide. *J. Am. Chem. Soc.* **1958**, *80*, 1339−1339.
(24) Wang, P.-p.; Sun, H.; Ji, Y.; Li, W.; Wang, X. Three-Dimensional Assembly of Single-Layered MoS2. *Adv. Mater.* **2014**, *26*, 964−969.
(25) Paek, S.-M.; Jung, H.; Park, M.; Lee, J.-K.; Choy, J.-H. An Inorganic Nanohybrid with High Specific Surface Area: TiO2-Pillared MoS2. *Chem. Mater.* **2005**, *17*, 3492−3498.
(26) Zhang, K.; Kim, H.-J.; Lee, J.-T.; Chang, G.-W.; Shi, X.; Kim, W.; Ma, M.; Kong, K.-j.; Choi, J.-M.; Song, M.-S.; Park, J. H. Unconventional Pore and Defect Generation in Molybdenum Disulfide: Application in High-Rate Lithium-Ion Batteries and the Hydrogen Evolution Reaction. *ChemSusChem* **2014**, *7*, 2489−2495.
(27) Yan, Y.; Xia, B.; Ge, X.; Liu, Z.; Wang, J.-Y.; Wang, X. Ultrathin MoS2 Nanoplates with Rich Active Sites as Highly Efficient Catalyst for Hydrogen Evolution. *ACS Appl. Mater. Interfaces* **2013**, *5*, 12794−12798.
(28) Cong, H.-P.; Ren, X.-C.; Wang, P.; Yu, S.-H. Macroscopic Multifunctional Graphene-Based Hydrogels and Aerogels by a Metal Ion Induced Self-Assembly Process. *ACS Nano* **2012**, *6*, 2693−2703.
(29) Goods, J. B.; Sydlik, S. A.; Walish, J. J.; Swager, T. M. Phosphate Functionalized Graphene with Tunable Mechanical Properties. *Adv. Mater.* **2014**, *26*, 718−723.
(30) Bo, Z.; Shuai, X.; Mao, S.; Yang, H.; Qian, J.; Chen, J.; Yan, J.; Cen, K. Green Preparation of Reduced Graphene Oxide for Sensing and Energy Storage Applications. *Sci. Rep.* **2014**, DOI: 10.1038/srep04684.
(31) Chang, Y.-H.; Wu, F.-Y.; Chen, T.-Y.; Hsu, C.-L.; Chen, C.-H.; Wiryo, F.; Wei, K.-H.; Chiang, C.-Y.; Li, L.-J. Three-Dimensional Molybdenum Sulfide Sponges for Electrocatalytic Water Splitting. *Small* **2014**, *10*, 895−900.
(32) Thomas, J. G. N. Kinetics of Electrolytic Hydrogen Evolution and the Adsorption of Hydrogen by Metals. *Trans. Faraday Soc.* **1961**, *57*, 1603−1611.
(33) Zhou, W.; Hou, D.; Sang, Y.; Yao, S. H.; Zhou, J.; Li, G.; Li, L.; Liu, H.; Chen, S. MoO2 Nanobelts@Nitrogen Self-Doped MoS2 Nanosheets as Effective Electrocatalysts for Hydrogen Evolution Reaction. *J. Mater. Chem. A* **2014**, *2*, 11358−11364.